Electric dipole polarizability of ^{58}Ni

I. Brandherm,[1] F. Bonaiti,[2,3,4] P. von Neumann-Cosel,[1,*] S. Bacca,[2] G. Colò,[5,6] G. R. Jansen,[7,4] Z. Z. Li (李征征),[8,9,10] H. Matsubara,[11,12] Y. F. Niu (牛一斐),[9,10] P.-G. Reinhard,[13] A. Richter,[1] X. Roca-Maza,[14,15,5,6] and A. Tamii[11]

[1]*Institut für Kernphysik, Technische Universität Darmstadt, D-64289 Darmstadt, Germany*
[2]*Institut für Kernphysik and PRISMA+ Cluster of Excellence, Johannes Gutenberg-Universität Mainz, D-55128 Mainz, Germany*
[3]*Facility for Rare Isotope Beams, Michigan State University, East Lansing, Michigan 48824, USA*
[4]*Physics Division, Oak Ridge National Laboratory, Oak Ridge, Tennessee 37831, USA*
[5]*Dipartimento di Fisica "Aldo Pontremoli", Università degli Studi di Milano, 20133 Milano, Italy*
[6]*INFN, Sezione di Milano, 20133 Milano, Italy*
[7]*National Center for Computational Sciences, Oak Ridge National Laboratory, Oak Ridge, Tennessee 37831, USA*
[8]*State Key Laboratory of Nuclear Physics and Technology, School of Physics, Peking University, Beijing 100871, China*
[9]*School of Nuclear Science and Technology, Lanzhou University, Lanzhou 730000, China*
[10]*Frontiers Science Center for Rare Isotope, Lanzhou University, Lanzhou 730000, China*
[11]*Research Center for Nuclear Physics, Osaka University, Ibaraki, Osaka 567-0047, Japan*
[12]*Faculty of Radiological Technology, Fujita Health University, Aichi 470-1192, Japan*
[13]*Institut für Theoretische Physik II, Universität Erlangen, D-91058 Erlangen, Germany*
[14]*Departament de Física Quàntica i Física, Martí i Franqués, 1, 08028 Barcelona, Spain*
[15]*Institut de Ciències del Cosmos, Universitat de Barcelona, Martí i Franqués, 1, 08028 Barcelona, Spain*

(Received 1 October 2024; accepted 10 January 2025; published 13 February 2025)

The electric dipole strength distribution in ^{58}Ni between 6 and 20 MeV has been determined from proton inelastic scattering experiments at very forward angles at RCNP, Osaka. The experimental data are rather well reproduced by quasiparticle random-phase approximation calculations including vibration coupling, despite a mild dependence on the adopted Skyrme interaction. They allow an estimate of the experimentally inaccessible high-energy contribution above 20 MeV, leading to an electric dipole polarizability $\alpha_{\mathrm{D}}(^{58}\mathrm{Ni}) = 3.48(31)$ fm^3. This serves as a test case for recent extensions of coupled-cluster calculations with chiral effective field theory interactions to nuclei with two nucleons on top of a closed-shell system.

DOI: 10.1103/PhysRevC.111.024312

I. INTRODUCTION

The nuclear equation of state (EOS) governs basic properties of nuclei [1] and neutron stars [2,3] as well as the dynamics of core-collapse supernovae [4] and neutron star mergers [5]. A systematic description of the EOS from nuclear densities to those in neutron stars is a central goal of current physics. A wealth of new data is available at high densities from observations on the properties of neutron stars and neutron star mergers but the present experimental constraints on the EOS around the saturation density n_0 of nuclear matter are still insufficient.

The EOS of symmetric nuclear matter is rather well constrained [1] in contrast to the properties of neutron-rich matter. The latter depends on the symmetry energy, which can be parametrized in an expansion around n_0 by the symmetry energy at saturation density $J(n_0)$ and its density dependence $L = 3n_0\partial J(n_0)/\partial n$. Higher-order terms are expected to be small. There are many experimental methods [6] providing constraints on J and L based on a model-dependent correlation between L and the neutron-skin thickness r_{skin} in nuclei with neutron excess [7–10]. For a recent summary, see Ref. [11]. The electric dipole polarizability, α_{D}, has also been identified as a key observable for constraining EOS parameters [9,12]. Proton inelastic scattering at incident energies of several hundred MeV at extreme forward angles has been developed as a new experimental tool exactly for the study of α_{D} [13] and results have been provided for a wide range of nuclei [14–18].

Two theoretical approaches have been used to describe α_{D} and derive constraints on the symmetry energy parameters: energy density functional theory (DFT) [1,19,20] and *ab initio* calculations [21–23] starting from chiral two- and three-nucleon interactions [24,25]. A correlation of the form $\alpha_{\mathrm{D}} \cdot J \propto L$, suggested by the droplet model, has been well studied in DFT [12,26]. In the *ab initio* context, comparing experimental determinations of α_D with theoretical predictions

*Contact author: vnc@ikp.tu-darmstadt.de

allows to validate constraints on nuclear matter properties from chiral forces.

In such efforts, coupled-cluster (CC) theory [21] plays a prominent role. Successful comparisons between CC predictions and experimental data in ^{40,48}Ca [16,18] and ^{68}Ni [27] have established this approach as an ideal tool to describe α_D in closed-shell, medium-mass nuclei. The same method has also been applied at the dripline to study the low-energy dipole strength and polarizability of ^{8}He [28,29]. Very recently, the reach of coupled-cluster calculations of α_D has been extended beyond closed-shell nuclei [30]. This new development has focused on two-particle-attached (2PA) systems, characterized by two nucleons outside a closed-shell nucleus. Combining closed-shell and 2PA coupled-cluster predictions, Ref. [30] enabled an analysis of the evolution of the dipole polarizability along the oxygen and calcium isotopic chains.

In this article, we present a measurement of the dipole polarizability of ^{58}Ni. Having two neutrons outside the doubly magic ^{56}Ni, it serves as a test case for the newly developed 2PA method. A study of ^{58}Ni is also of interest to systematically explore the theoretically predicted dependence on neutron skin thickness when combined with data for ^{64}Ni (presently under analysis) and ^{68}Ni [31].

II. EXPERIMENT

The ^{58}Ni(p, p') reaction has been measured at RCNP, Osaka, at an incident proton energy of 295 MeV in a laboratory scattering angle range 0.4°–5.15° and for excitation energies in the range 5–25 MeV. An energy resolution of 22 keV (full width at half-maximum) was achieved applying dispersion matching techniques. The experimental techniques and the raw data analysis are described in Ref. [32]. Further details of the ^{58}Ni experiment are described in Ref. [33] presenting a state-by-state analysis of electric and magnetic dipole transitions for excitation energies up to 13 MeV. These data provide information on the isovector spin-flip $M1$ resonance and candidates for a toroidal $E1$ mode in nuclei [34].

The top panel of Fig. 1 presents representative energy spectra measured at laboratory scattering angles $\Theta_{\text{lab}} = 0.40°, 2.38°$, and 5.15°. The cross sections above 10 MeV show a broad resonance with a maximum at about 18 MeV and cross sections strongly decreasing with scattering angle. The angular dependence is consistent with relativistic Coulomb excitation of $E1$ transitions. Thus, we identify this resonance structure as the isovector giant dipole resonance (IVGDR).

The various contributions to the spectra were separated using a multipole decomposition analysis (MDA) as described, e.g., in Ref. [35]. Theoretical angular distributions for the relevant multipoles were obtained from distorted wave Born approximation calculations with transition amplitudes from quasiparticle-phonon-model calculations, cf. Ref. [33]. Since only spectra at seven angles were available, the number of multipoles that can be considered in the MDA was limited. Following the method described in Refs. [35,36] and using the experimental $E0$ and $E2$ strength distributions in ^{58}Ni from inelastic α scattering [37], the contributions to the spectra due to excitation of the isoscalar giant monopole (ISGMR)

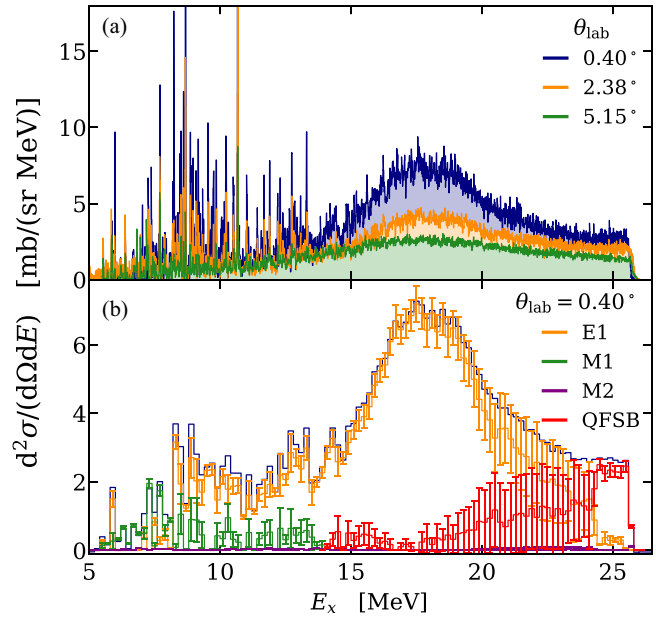

FIG. 1. (a) Spectra of the ^{58}Ni(p, p') reaction at $E_0 = 295$ MeV and scattering angles $\Theta_{\text{lab}} = 0.40°$, 2.38°, and 5.15°. (b) Example of the MDA of the spectrum at $\Theta_{\text{lab}} = 0.4°$ in 200 keV bins (blue) and decomposition into contributions of $E1$ (orange), $M1$ (green), multipoles $\lambda > 1$ (purple), and an empirical background (red). Contributions from the ISGMR and ISGQR were subtracted prior to the MDA as described in the text.

and quadrupole (ISGQR) resonances were subtracted prior to the MDA. Additionally, an empirical background (most likely due to quasifree scattering) was considered. Its angular dependence was taken from experiments on heavier nuclei [14,35], which showed a momentum-transfer dependence approximately independent of nuclear mass.

Results for the most forward angle measured are presented in the bottom part of Fig. 1 as example, where the spectra was rebinned to 200 keV. $E1$ cross sections dominate over the whole excitation energy range. At energies up to 13.5 MeV, the spin-flip $M1$ resonance makes sizable contributions. The two strongest $M1$ transitions (cf. Ref. [33]) were subtracted by hand because they lead to large uncertainties in the MDA for the respective energy bins. The background becomes relevant on the high-energy flank of the IVGDR. Above 20 MeV, the uncertainties of the $E1$/background decomposition become very large due to the similarity of their angular distributions. Contributions from higher multipoles are negligibly small.

III. EXTRACTION OF THE DIPOLE POLARIZABILITY

The $E1$ cross sections resulting from the MDA were converted into equivalent photoabsorption cross sections using the virtual photon method [40]. The virtual photon spectrum was calculated in an eikonal approach [41] to Coulomb excitation, integrated over the distribution of scattering angles covered in the solid angle of each angular bin as described in Ref. [35]. The resulting photoabsorption cross sections are displayed as blue circles in Fig. 2(a).

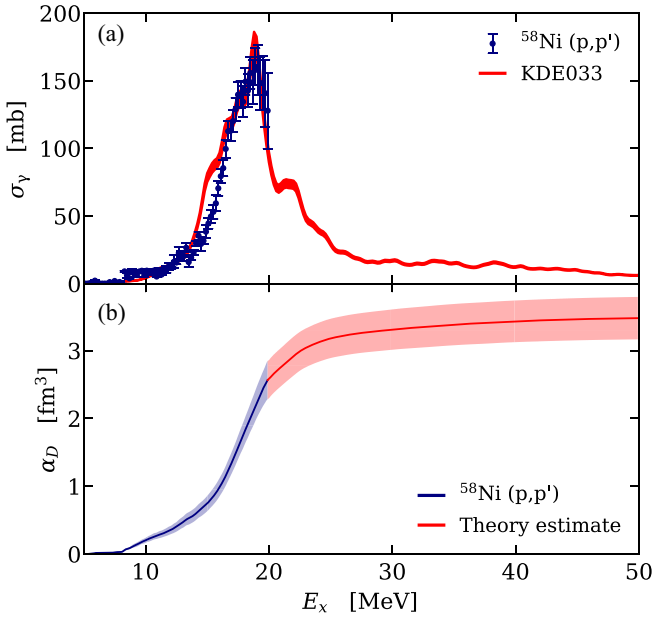

FIG. 2. (a) Photoabsorption cross sections of ^{58}Ni derived from the spectrum at a scattering angle of 0.40° using the virtual photon method (blue circles). The red curve shows a QRPA calculation including qPVC [38] with the KDE033 interaction [39] normalized to the data. (b) Electric dipole polarizability α_D derived from the photoabsorption cross sections. The blue and red bands band show the present data and the contribution at excitation energies >20 MeV based on the theoretical estimate explained in the text with their uncertainties, respectively.

The electric dipole polarizability α_D is related to the photoabsorption cross sections by

$$\alpha_{\mathrm{D}} = \frac{\hbar c}{2\pi^2} \int \frac{\sigma_\gamma}{E_{\mathrm{x}}^2} \mathrm{d}E_{\mathrm{x}}. \tag{1}$$

The experimental result for the energy region 6–20 MeV is plotted as blue curve in Fig. 2(b) and amounts to $\alpha_{\mathrm{D}} = 2.57(28)$ fm^3. The uncertainty band considers the systematic errors of the experimental cross sections (cf. Ref. [33]) and the MDA (as described in Ref. [35]). Statistical uncertainties are negligible.

Photoabsorption data from the (γ, xn) reaction are available for excitation energies up to 33 MeV [42], but in contrast to heavy nuclei the unknown (γ, p) channel is expected to be significant. Thus, α_{D} contributions at energies $E_{\mathrm{x}} > 20$ MeV were estimated with a theory-aided procedure using energy density functionals. Previous analyses of this type [17,31] were based on the folding of quasiparticle random-phase approximaton (QRPA) calculations with interactions reproducing the IVGDR centroid with a Lorentzian fitted to the experimental data. Here, we go beyond and include quasiparticle vibration coupling (qPVC) which has recently been shown to permit not only a reproduction of the width of the ISGMR [38,43], but also resolve the discrepancies between ^{208}Pb and lighter nuclei in theoretical attempts to extract the compressibility from the energy centroid of the ISGMR [44].

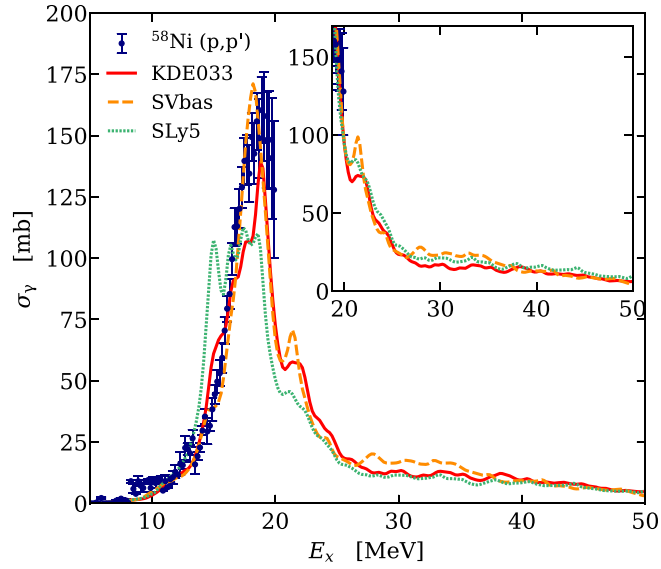

FIG. 3. Photoabsorption cross sections of ^{58}Ni from the present work compared with QRPA calculations including qPVC [38], based on the KDE033 (solid red line) [39], SV-bas (dashed orange line) [45], and SLy5 (short-dashed green line) [46] interactions. The inset shows the high-energy flanks normalized to each other at 20 MeV.

QRPA calculations including qPVC with the approach described in Ref. [38] are shown in Fig. 3 for Skyrme forces KDE033 [39], SV-bas [45], and SLy5 [46]. The photoabsorption cross sections predicted with KDE033 (solid red line) provide a very good description of the centroid and width of the IVGDR, but the total strength is somewhat underestimated. Calculations with SV-bas (dashed orange line) give a similar width and reproduce the maximum cross section, but the centroid energy is about 1 MeV too low. Finally, the SLy5 result (short-dashed green line) shows a much stronger fragmentation and an even lower energy centroid. Since all calculations require an adjustment to the data, the absolute values of the different models for the high-energy (>20 MeV) contribution to the polarizability becomes very dependent on the assumptions made in the normalization procedure.

For a quantitative estimate of the high-energy contribution to the polarizability, we choose a normalization to the results obtained with the KDE033 interaction. As illustrated in Fig. 2(a), it provides a very good description of the IVGDR after adjusting the absolute height. The corresponding contribution to the polarizability for excitation energies >20 MeV is displayed in Fig. 2(b) as red curve. The polarizability is integrated up to 50 MeV, where saturation is reached.

The model dependence due to the choice of specific interactions is estimated from the variation of the three calculations after normalization to each other at 20 MeV. As demonstrated in the inset of Fig. 3, then the theoretically predicted high-energy tails become similar in shape and magnitude. The similar energy dependence might look surprising at first sight but can be understood from the following argument: structures on the low-energy side of the IVGDR are related to the coupling to individual collective phonons, which leads to the phenomenon of fine structure [47,48]. At higher excitation

energies stochastic coupling [49] predominates, i.e., the strength distribution is mainly determined by the density of states and an average coupling matrix element between the particle-hole and more complex states.

The theoretically predicted contribution to the polarizability amounts to $\alpha_{\rm D}(E_{\rm x} > 20\,{\rm MeV}) = 0.91$ fm^3 with an uncertainty of 0.04 fm^3 due to the normalization. As pointed above, a model-dependent error is estimated from the variation of the three calculations (0.13 fm^3). The parameter dependence of the individual calculations for the different forces was estimated from variations of the cutoff energy of the single-particle spectrum and the minimum strength of phonons considered in the qPVC and found to be negligibly small. Assuming that all above-discussed error contributions are independent, we find for the dipole polarizability $\alpha_{\rm D}(^{58}{\rm Ni}) = 3.48(31)$ fm^3.

IV. COUPLED-CLUSTER CALCULATIONS

The electric dipole polarizability of Eq. (1) is a sum rule of the photoabsorption cross section, which can be itself written in terms of the dipole response function

$$R(E_{\rm x}) = \sum_{\mu} |\,\langle\Psi_\mu|\Theta|\Psi_0\rangle\,|^2 \delta(E_\mu - E_0 - E_{\rm x})\,, \qquad (2)$$

where $|\Psi_0\rangle$ and $|\Psi_\mu\rangle$ are ground and excited state of the nucleus with energies E_0 and E_μ, respectively, while Θ is the dipole operator. The sum over μ in Eq. (2) runs over bound and continuum excited states of the nucleus. This makes the calculation of response functions particularly challenging, because of the presence of unbound configurations arising from the break-up of the nucleus into fragments. To avoid this, one can resort to the Lorentz integral transform (LIT) method [50], which is based on an integral transform of the response function with a Lorentzian kernel as

$$L(\sigma,\Gamma) = \frac{\Gamma}{\pi}\int dE_{\rm x}\,\frac{R(E_{\rm x})}{(E_{\rm x}-\sigma)^2+\Gamma^2}. \qquad (3)$$

Calculating the latter requires "only" the solution of a bound-state problem. Because the Lorentzian kernel tends to a Dirac delta function as $\Gamma \to 0$, one has that

$$L(\sigma,\Gamma\to 0) = \int dE_{\rm x}\,R(E_{\rm x})\delta(E_{\rm x}-\sigma) = R(\sigma)\,, \qquad (4)$$

which effectively means that in this limit the LIT becomes the response function, where the variable $E_{\rm x}$ is renamed to σ. Such a response function is discretized in the sense that excited states in the continuum are represented by bound pseudostates. Nevertheless, Eq. (4) can be used to compute the nth moments from the response function as

$$m_n = \int dE_{\rm x}\,E_{\rm x}^n\,R(E_{\rm x}) = \int d\sigma\,\sigma^n L(\sigma,\Gamma\to 0)\,. \qquad (5)$$

Given that sum rules can be written as expectation values on the ground state, the utilization of bound pseudostates in such a calculation is mathematically valid [51]. With this reasoning, the electric dipole polarizability is simply related to the inverse energy-weighted sum rule of the dipole response function as $\alpha_{\rm D} = 2\alpha\hbar c m_{-1}$, where m_{-1} is calculated using Eq. (5), and α is the fine structure constant.

Merging the LIT approach [50] with the coupled-cluster theory [52] for closed-(sub)shell nuclei led to a method dubbed LIT-CC, which is based on the following steps [53]. First, the ground state is constructed starting from a Slater determinant (Φ_0) and imprinting correlations on top of it via an exponential ansatz $|\Psi_0\rangle = e^T\,|\Phi_0\rangle$. The cluster operator T can be expanded in terms of a sum of n-particle–n-hole excitations. Second, the Hamiltonian and the excitation operator are similarity transformed to $\overline{H} = e^{-T}He^T$ and $\overline{\Theta} = e^{-T}\Theta e^T$, respectively. Third, excited states of a closed-(sub)shell nucleus are computed as $|\Psi_\mu\rangle = R_\mu e^T\,|\Phi_0\rangle$, where the operator R_μ is also expanded in terms of particle-hole excitations, by solving an equation of motion. Finally, α_D can be computed with the prescription described above.

While the LIT-CC method has been very successfully used for closed-shell nuclei [16,18,21,22,28,53,54], recently it has been extended to nuclei that have two nucleons on top of a closed shell system using the two-particle attached (2PA) technique [30]. In this case, excited states of 2PA nuclei can be obtained with the following ansatz:

$$\left|\Psi_\mu^{(\rm A+2)}\right\rangle = R_\mu^{A+2}\left|\Psi_0^{(A)}\right\rangle = R_\mu^{A+2}e^T\left|\Phi_0^{(A)}\right\rangle, \qquad (6)$$

where A is the mass number of the closed-(sub)shell system and the excitation operator R_μ^{A+2} involves the net creation of the two extra nucleons on top of the closed-(sub)shell system

$$R_\mu^{A+2} = \frac{1}{2}\sum_{ab} r_\mu^{ab}a_a^\dagger a_b^\dagger + \frac{1}{6}\sum_{abci} r_{i,\mu}^{abc}a_a^\dagger a_b^\dagger a_c^\dagger a_i\,. \qquad (7)$$

In this work we adopt the particle-hole expansion of Eq. (7), including two-particle zero-hole (2p-0h) and three-particle one-hole (3p-1h) contributions. The addition of higher-order terms is at the moment prohibitive. In Ref. [30], this method was employed to study α_D in oxygen and calcium isotopes. Here, we apply it to a larger mass number by studying the ^{58}Ni nucleus, starting from the ^{56}Ni closed-shell neighbor.

We perform our calculation using the chiral nucleon-nucleon and three-nucleon interactions 1.8/2.0 (EM) [24], ΔNLO$_{\rm GO}$(450), and ΔNNLO$_{\rm GO}$(450) [55]. The chiral force 1.8/2.0 (EM) yields accurate binding energies in medium-mass and heavy nuclei [56], and it contains two-nucleon forces up to next-to-next-to-next-to-leading order, softened via similarity renormalization group transformation at a scale of 1.8 fm^{-1}, and three-nucleon forces at next-to-next-to-leading order, with a momentum cutoff of 2.0 fm^{-1}. The interactions ΔNLO$_{\rm GO}$(450) and ΔNNLO$_{\rm GO}$(450) contain the Δ isobar as an explicit degree of freedom, and they are given at next-to-leading order and next-to-next-to-leading order, respectively.

Our 2PA calculations of α_D start from an Hartree-Fock reference state, expanded on a harmonic oscillator basis of up to 13 major shells. We studied the convergence of our results varying the underlying harmonic oscillator frequency $\hbar\Omega$ between 12 and 16 MeV. An additional energy cut at $E_{3,\rm max} = 16\hbar\Omega$ is applied on three-body contributions.

In Fig. 4, in the upper panel we show the discretized response function versus the excitation energy calculated with

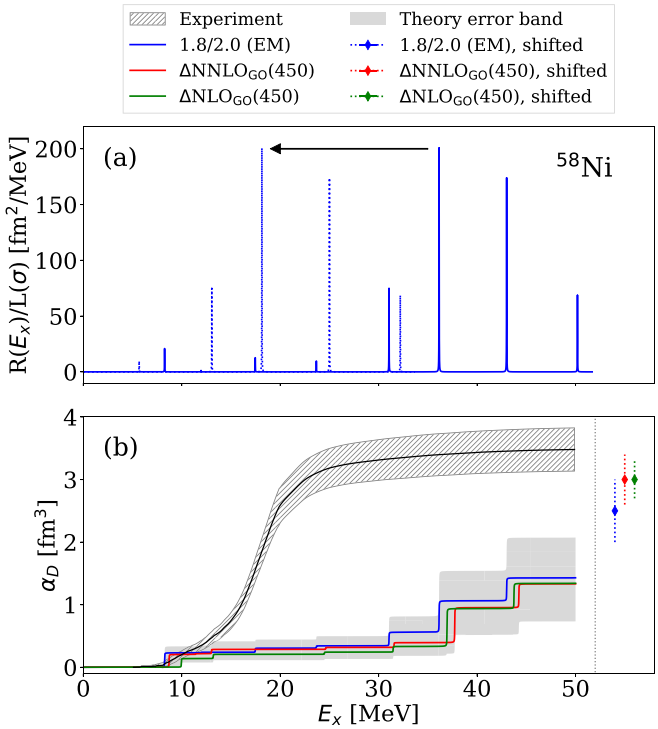

FIG. 4. (a) Discretized response function of ^{58}Ni calculated with the 1.8/2.0 (EM) interaction (solid line), and the corresponding curve obtained shifting the response to the experimental IVGDR energy of 18 MeV (dotted line). (b) α_D running sums for the 1.8/2.0 (EM) and Δ-full interaction models, in comparison to experiment. α_D predictions obtained by shifting the response to the experimental IVGDR energy are shown on the right-hand side as diamonds with dotted error bars.

the 1.8/2.0 (EM) interaction. We clearly see one peak located below 10 MeV, while the four largest peaks which constitute the IVGDR are found at high energy, beyond 30 MeV. In the lower panel we compare instead the theoretical and experimental running sum rules, defined as in Eq. (1), where the integral is performed up to a maximum upper limit, which is varied from 0 to 50 MeV. The experimental data are shown with a hatched band, while in case of the theoretical results, we present three different interactions: the 1.8/2.0 (EM) in blue, the ΔNLO$_{GO}$(450) and ΔNNLO$_{GO}$(450) in green and red, respectively.

Interestingly, we see that experiment and theory agree with each other at low energy. Considering the interaction dependence and the many-body truncation error, estimated according to the recipe devised in Ref. [30], we find $0.1 < \alpha_D < 0.3$ fm^3 below 11 MeV of excitation energy, in good accordance with the corresponding experimental result of $0.2 < \alpha_D < 0.3$ fm^3 obtained from the MDA analysis. At higher energies, however, the rise of the experimental running sum rule is much faster than that of the theoretical calculations. The reason for this behavior lies in the fact that the IVGDR pseudostates are found at higher energies with respect to the experiment, approximately 20 MeV too high. We have already observed such effect in other isotope chains [30] and it is most likely related with the truncation of Eq. (7) at the 3p-1h level, which does not grasp all the necessary correlations. To gauge the possible role of missing higher-order correlations, we can compare the share of the pseudostates' norm in 2p-0h configurations to the corresponding total norm. As a rule of thumb, if the 2p-0h contribution to the norm is around 90%, the nuclear state of interest has a simple 2PA structure and an accurate description of it can be achieved employing the 3p-1h approximation [57,58]. In the case of ^{58}Ni, the 2p-0h contribution to the total norm is above 70% for the first excited states at around 10 MeV, where the theoretical running sum agrees with experiment. At higher energies, instead, it falls quickly below 50%, suggesting the need of higher order contributions to the 2PA expansion. This is reflected by the extent of the theoretical error band shown in grey. It contains the many-body truncation uncertainty, which is clearly dominating over the potential dependence indicated by the difference of the three colored curves.

In order to check that the major rise of the experimental running sum is given by the IVGDR states, we took the theoretical discretized response functions and shifted all peaks by around 20 MeV, so that for each interaction the largest peak is located at the same energy as the experimental IVGDR. By doing so, α_D is clearly enhanced to a value compatible with the experimental result, as shown by the dotted error bars at the right of the lower panel of Fig. 4.

V. CONCLUSIONS

We have determined the electric dipole polarizability of ^{58}Ni from 295 MeV inelastic proton scattering experiments at very forward angles. The extraction is limited to an excitation energy of 20 MeV due to the quasifree continuum background which shows a similar angular distribution as the Coulomb excitation cross sections. QRPA calculations including qPVC provide a good description of the energy centroid and width of the IVGDR in ^{58}Ni, permitting an estimate of the experimentally inaccessible strength above 20 MeV.

The resulting value of α_D serves as a test case for *ab initio*–based coupled cluster calculations with the newly developed 2PA method to describe nuclei with two particles outside closed-shell systems. At the present level of the CC expansion the low-energy $E1$ strength can be predicted well, but the IVGDR is found at an excitation energy about 20 MeV too high resulting in correspondingly small theoretical α_D values. This points to the need for higher order many-body correlations in the 2PA expansion in order to achieve a more accurate description of the IVGDR contribution to the polarizability. To address this issue, alternative approaches could also be pursued in the future, such as coupling the LIT method to coupled-cluster calculations employing axially symmetric reference states [59–62].

ACKNOWLEDGMENTS

This work was supported by the Deutsche Forschungsgemeinschaft (DFG, German Research Foundation) – Project-ID 279384907 – SFB 1245 and through the Cluster of Excellence "Precision Physics, Fundamental Interactions, and Structure of Matter" (PRISMA$^+$ EXC 2118/1, Project ID

39083149), and by the U.S. Department of Energy, Office of Science, Office of Advanced Scientific Computing Research and Office of Nuclear Physics, Scientific Discovery through Advanced Computing (SciDAC) program (SciDAC-5 NUCLEI) and Office of Nuclear Physics, under the FRIB Theory Alliance Award No. DE-SC0013617. This research used resources of the Oak Ridge Leadership Computing Facility located at Oak Ridge National Laboratory, which is supported by the Office of Science of the Department of Energy under Contract No. DE-AC05-00OR22725. Computer time was provided by the Innovative and Novel Computational Impact on Theory and Experiment (INCITE) program and by the supercomputer Mogon at Johannes Gutenberg Universität Mainz. X.R.-M. acknowledges support by Grant No. PID2020-118758GB-I00 funded by MCIN/AEI/10.13039/501100011033; by the "Unit of Excellence María de Maeztu 2020–2023" award to the Institute of Cosmos Sciences, Grant No. CEX2019-000918-M funded by MCIN/AEI/10.13039/501100011033; and by the Generalitat de Catalunya, Grant No. 2021SGR01095. Y.F.N. acknowledges funding from National Key Research and Development (R&D) Program under Grant No. 2021YFA1601500 and Natural Science Foundation of China under Grant No. 12075104. P.-G.R. acknowledges supply of computing resources from the RRZE of the Friedrich-Alexander university Erlangen/Nürnberg.

This manuscript has been authored, in part, by UTBattelle, LLC, under Contract No. DE-AC05-00OR22725 with the U.S. Department of Energy (DOE). The US government retains and the publisher, by accepting the article for publication, acknowledges that the U.S. government retains a nonexclusive, paid-up, irrevocable, worldwide license to publish or reproduce the published form of this manuscript, or allow others to do so, for U.S. government purposes. DOE will provide public access to these results of federally sponsored research in accordance with the DOE Public Access Plan [63].

[1] X. Roca-Maza and N. Paar, Nuclear equation of state from ground and collective excited state properties of nuclei, Prog. Part. Nucl. Phys. **101**, 96 (2018).

[2] J. Lattimer, Neutron stars and the nuclear matter equation of state, Annu. Rev. Nucl. Part. Sci. **71**, 433 (2021).

[3] S. Huth, P. T. H. Pang, I. Tews, T. Dietrich, A. Le Fèvre, A. Schwenk, W. Trautmann, K. Agarwal, M. Bulla, M. W. Coughlin, and C. Van Den Broeck, Constraining neutron-star matter with microscopic and macroscopic collisions, Nature (London) **606**, 276 (2022).

[4] H. Yasin, S. Schäfer, A. Arcones, and A. Schwenk, Equation of state effects in core-collapse supernovae, Phys. Rev. Lett. **124**, 092701 (2020).

[5] G. Raaijmakers, S. K. Greif, K. Hebeler, T. Hinderer, S. Nissanke, A. Schwenk, T. E. Riley, A. L. Watts, J. M. Lattimer, and W. C. G. Ho, Constraints on the dense matter equation of state and neutron star properties from NICER's mass-radius estimate of PSR J0740+6620 and multimessenger observations, Astrophys. J. Lett. **918**, L29 (2021).

[6] M. Thiel, C. Sfienti, J. Piekarewicz, C. J. Horowitz, and M. Vanderhaeghen, Neutron skins of atomic nuclei: Per aspera ad astra, J. Phys. G: Nucl. Part. Phys. **46**, 093003 (2019).

[7] B. A. Brown, Neutron radii in nuclei and the neutron equation of state, Phys. Rev. Lett. **85**, 5296 (2000).

[8] M. Centelles, X. Roca-Maza, X. Viñas, and M. Warda, Nuclear symmetry energy probed by neutron skin thickness of nuclei, Phys. Rev. Lett. **102**, 122502 (2009).

[9] P.-G. Reinhard and W. Nazarewicz, Information content of a new observable: The case of the nuclear neutron skin, Phys. Rev. C **81**, 051303(R) (2010).

[10] X. Roca-Maza, M. Centelles, X. Viñas, and M. Warda, Neutron skin of ^{208}Pb, nuclear symmetry energy, and the parity radius experiment, Phys. Rev. Lett. **106**, 252501 (2011).

[11] J. M. Lattimer, Constraints on nuclear symmetry energy parameters, Particles **6**, 30 (2023).

[12] X. Roca-Maza, M. Brenna, G. Colò, M. Centelles, X. Viñas, B. K. Agrawal, N. Paar, D. Vretenar, and J. Piekarewicz, Electric dipole polarizability in ^{208}Pb: Insights from the droplet model, Phys. Rev. C **88**, 024316 (2013).

[13] P. von Neumann-Cosel and A. Tamii, Electric and magnetic dipole modes in high-resolution inelastic proton scattering at 0°, Eur. Phys. J. A **55**, 110 (2019).

[14] A. Tamii *et al.*, Complete electric dipole response and the neutron skin in ^{208}Pb, Phys. Rev. Lett. **107**, 062502 (2011).

[15] T. Hashimoto, A.M. Krumbholz, P.G. Reinhard, A. Tamii, P. von Neumann-Cosel, T. Adachi, N. Aoi, C.A. Bertulani, H. Fujita, Y. Fujita, E. Ganioglu, K. Hatanaka, E. Ideguchi, C. Iwamoto, T. Kawabata, N. T. Khai, A. Krugmann, D. Martin, H. Matsubara, K. Miki *et al.*, Dipole polarizability of ^{120}Sn and nuclear energy density functionals, Phys. Rev. C **92**, 031305(R) (2015).

[16] J. Birkhan, M. Miorelli, S. Bacca, S. Bassauer, C. A. Bertulani, G. Hagen, H. Matsubara, P. von Neumann-Cosel, T. Papenbrock, N. Pietralla, V. Y. Ponomarev, A. Richter, A. Schwenk, and A. Tamii, Electric dipole polarizability of ^{48}Ca and implications for the neutron skin, Phys. Rev. Lett. **118**, 252501 (2017).

[17] S. Bassauer *et al.*, Evolution of the dipole polarizability in the stable tin isotope chain, Phys. Lett. B **810**, 135804 (2020).

[18] R. W. Fearick, P. von Neumann-Cosel, S. Bacca, J. Birkhan, F. Bonaiti, I. Brandherm, G. Hagen, H. Matsubara, W. Nazarewicz, N. Pietralla, V. Y. Ponomarev, P.-G. Reinhard, X. Roca-Maza, A. Richter, A. Schwenk, J. Simonis, and A. Tamii, Electric dipole polarizability of ^{40}Ca, Phys. Rev. Res. **5**, L022044 (2023).

[19] M. Bender, P.-H. Heenen, and P.-G. Reinhard, Self-consistent mean-field models for nuclear structure, Rev. Mod. Phys. **75**, 121 (2003).

[20] J. Piekarewicz, B. K. Agrawal, G. Colò, W. Nazarewicz, N. Paar, P.-G. Reinhard, X. Roca-Maza, and D. Vretenar, Electric dipole polarizability and the neutron skin, Phys. Rev. C **85**, 041302(R) (2012).

[21] G. Hagen, A. Ekström, C. Forssén, G. R. Jansen, W. Nazarewicz, T. Papenbrock, K. A. Wendt, S. Bacca, N. Barnea, B. Carlsson, C. Drischler, K. Hebeler, M. Hjorth-Jensen, M.

Miorelli, G. Orlandini, A. Schwenk, and J. Simonis, Neutron and weak-charge distributions of the ^{48}Ca nucleus, Nat. Phys. **12**, 186 (2016).

[22] J. Simonis, S. Bacca, and G. Hagen, First principles electromagnetic responses in medium-mass nuclei, Eur. Phys. J. A **55**, 241 (2019).

[23] B. Hu, W. Jiang, T. Miyagi, Z. Sun, A. Ekström, C. Forssén, G. Hagen, J. D. Holt, T. Papenbrock, S. R. Stroberg, and I. Vernon, Ab initio predictions link the neutron skin of ^{208}Pb to nuclear forces, Nat. Phys. **18**, 1196 (2022).

[24] K. Hebeler, S. K. Bogner, R. J. Furnstahl, A. Nogga, and A. Schwenk, Improved nuclear matter calculations from chiral low-momentum interactions, Phys. Rev. C **83**, 031301(R) (2011).

[25] A. Ekström, G. R. Jansen, K. A. Wendt, G. Hagen, T. Papenbrock, B. D. Carlsson, C. Forssén, M. Hjorth-Jensen, P. Navrátil, and W. Nazarewicz, Accurate nuclear radii and binding energies from a chiral interaction, Phys. Rev. C **91**, 051301(R) (2015).

[26] X. Roca-Maza, X. Viñas, M. Centelles, B. K. Agrawal, G. Colò, N. Paar, J. Piekarewicz, and D. Vretenar, Neutron skin thickness from the measured electric dipole polarizability in ^{68}Ni, ^{120}Sn, and ^{208}Pb, Phys. Rev. C **92**, 064304 (2015).

[27] S. Kaufmann *et al.*, Charge radius of the short-lived ^{68}Ni and correlation with the dipole polarizability, Phys. Rev. Lett. **124**, 132502 (2020).

[28] F. Bonaiti, S. Bacca, and G. Hagen, Ab initio coupled-cluster calculations of ground and dipole excited states in ^{8}He, Phys. Rev. C **105**, 034313 (2022).

[29] F. Bonaiti and S. Bacca, Low-energy dipole strength in ^{8}He, Few-Body Syst. **65**, 54 (2024).

[30] F. Bonaiti, S. Bacca, G. Hagen, and G. R. Jansen, Electromagnetic observables of open-shell nuclei from coupled-cluster theory, Phys. Rev. C **110**, 044306 (2024).

[31] D. M. Rossi *et al.*, Measurement of the dipole polarizability of the unstable neutron-rich nucleus ^{68}Ni, Phys. Rev. Lett. **111**, 242503 (2013).

[32] A. Tamii *et al.*, Measurement of high energy resolution inelastic proton scattering at and close to zero degrees, Nucl. Instrum. Methods Phys. Res. A **605**, 326 (2009).

[33] I. Brandherm, P. von Neumann-Cosel, R. Mancino, G. Martínez-Pinedo, H. Matsubara, V. Y. Ponomarev, A. Richter, M. Scheck, and A. Tamii, Electric and magnetic dipole strength in ^{58}Ni from forward-angle proton scattering, Phys. Rev. C **110**, 034319 (2024).

[34] P. von Neumann-Cosel, V. O. Nesterenko, I. Brandherm, P. I. Vishnevskiy, P.-G. Reinhard, J. Kvasil, H. Matsubara, A. Repko, A. Richter, M. Scheck, and A. Tamii, Candidate toroidal electric dipole mode in the spherical nucleus ^{58}Ni, Phys. Rev. Lett. **133**, 232502 (2024).

[35] S. Bassauer *et al.*, Electric and magnetic dipole strength in ^{112,114,116,118,120,124}Sn, Phys. Rev. C **102**, 034327 (2020).

[36] L. M. Donaldson *et al.*, Deformation dependence of the isovector giant dipole resonance: The neodymium isotopic chain revisited, Phys. Lett. B **776**, 133 (2018).

[37] Y.-W. Lui, D. H. Youngblood, H. L. Clark, Y. Tokimoto, and B. John, Isoscalar giant resonances for nuclei with mass between 56 and 60, Phys. Rev. C **73**, 014314 (2006).

[38] Z. Z. Li, Y. F. Niu, and G. Colò, Toward a unified description of isoscalar giant monopole resonances in a self-consistent quasiparticle-vibration coupling approach, Phys. Rev. Lett. **131**, 082501 (2023).

[39] B. K. Agrawal, S. Shlomo, and V. K. Au, Determination of the parameters of a Skyrme type effective interaction using the simulated annealing approach, Phys. Rev. C **72**, 014310 (2005).

[40] C. A. Bertulani and G. Baur, Electromagnetic processes in relativistic heavy ion collisions, Phys. Rep. **163**, 299 (1988).

[41] C. A. Bertulani and A. M. Nathan, Excitation and photon decay of giant resonances from high-energy collisions of heavy ions, Nucl. Phys. A **554**, 158 (1993).

[42] S. C. Fultz, R. A. Alvarez, B. L. Berman, and P. Meyer, Photoneutron cross sections of ^{58}Ni and ^{60}Ni, Phys. Rev. C **10**, 608 (1974).

[43] E. Litvinova, Relativistic approach to the nuclear breathing mode, Phys. Rev. C **107**, L041302 (2023).

[44] U. Garg and G. Colò, The compression-mode giant resonances and nuclear incompressibility, Prog. Part. Nucl. Phys. **101**, 55 (2018).

[45] P. Klüpfel, P.-G. Reinhard, T. J. Bürvenich, and J. A. Maruhn, Variations on a theme by Skyrme: A systematic study of adjustments of model parameters, Phys. Rev. C **79**, 034310 (2009).

[46] E. Chabanat, P. Bonche, P. Haensel, J. Meyer, and R. Schaeffer, A Skyrme parametrization from subnuclear to neutron star densities, Nucl. Phys. A **627**, 710 (1997).

[47] I. Poltoratska, R. W. Fearick, A. M. Krumbholz, E. Litvinova, H. Matsubara, P. von Neumann-Cosel, V. Y. Ponomarev, A. Richter, and A. Tamii, Fine structure of the isovector giant dipole resonance in ^{208}Pb: Characteristic scales and level densities, Phys. Rev. C **89**, 054322 (2014).

[48] J. Carter *et al.*, Damping of the isovector giant dipole resonance in ^{40,48}Ca, Phys. Lett. B **833**, 137374 (2022).

[49] P. von Neumann-Cosel, V. Y. Ponomarev, A. Richter, and J. Wambach, Gross, intermediate and fine structure of nuclear giant resonances: Evidence for doorway states, Eur. Phys. J. A **55**, 224 (2019).

[50] V. D. Efros, W. Leidemann, G. Orlandini, and N. Barnea, The Lorentz integral transform (LIT) method and its applications to perturbation-induced reactions, J. Phys. G: Nucl. Part. Phys. **34**, R459 (2007).

[51] N. Nevo Dinur, N. Barnea, C. Ji, and S. Bacca, Efficient method for evaluating energy-dependent sum rules, Phys. Rev. C **89**, 064317 (2014).

[52] G. Hagen, T. Papenbrock, M. Hjorth-Jensen, and D. J. Dean, Coupled-cluster computations of atomic nuclei, Rep. Prog. Phys. **77**, 096302 (2014).

[53] S. Bacca, N. Barnea, G. Hagen, G. Orlandini, and T. Papenbrock, First principles description of the giant dipole resonance in ^{16}O, Phys. Rev. Lett. **111**, 122502 (2013).

[54] M. Miorelli, S. Bacca, G. Hagen, and T. Papenbrock, Computing the dipole polarizability of ^{48}Ca with increased precision, Phys. Rev. C **98**, 014324 (2018).

[55] W. G. Jiang, A. Ekström, C. Forssén, G. Hagen, G. R. Jansen, and T. Papenbrock, Accurate bulk properties of nuclei from $a = 2$ to ∞ from potentials with Δ isobars, Phys. Rev. C **102**, 054301 (2020).

[56] J. Simonis, S. R. Stroberg, K. Hebeler, J. D. Holt, and A. Schwenk, Saturation with chiral interactions and consequences for finite nuclei, Phys. Rev. C **96**, 014303 (2017).

[57] G. R. Jansen, M. Hjorth-Jensen, G. Hagen, and T. Papenbrock, Toward open-shell nuclei with coupled-cluster theory, Phys. Rev. C **83**, 054306 (2011).

[58] G. R. Jansen, Spherical coupled-cluster theory for open-shell nuclei, Phys. Rev. C **88**, 024305 (2013).

[59] S. J. Novario, G. Hagen, G. R. Jansen, and T. Papenbrock, Charge radii of exotic neon and magnesium isotopes, Phys. Rev. C **102**, 051303(R) (2020).

[60] G. Hagen, S. J. Novario, Z. H. Sun, T. Papenbrock, G. R. Jansen, J. G. Lietz, T. Duguet, and A. Tichai, Angular-momentum projection in coupled-cluster theory: Structure of ^{34}Mg, Phys. Rev. C **105**, 064311 (2022).

[61] Z. H. Sun, A. Ekström, C. Forssén, G. Hagen, G. R. Jansen, and T. Papenbrock, Multiscale physics of atomic nuclei from first principles, arXiv:2404.00058.

[62] B. S. Hu, Z. H. Sun, G. Hagen, and T. Papenbrock, *Ab initio* computations of strongly deformed nuclei near ^{80}Zr, Phys. Rev. C **110**, L011302 (2024).

[63] https://www.energy.gov/doe-public-access-plan